Electronic Supplementary Information for "Thermodynamic stability and reactivity of amorphised tricalcium silicate"

Alastair T. M. Marsh [a*], Thiago R. S. Nobre [b], Marjorie Etchevers [a], Alexander Pisch [c], Karen L. Scrivener [a]

[a] Laboratory of Construction Materials, École Polytechnique Fédérale de Lausanne, Lausanne 1015, Switzerland

[b] Department of Construction Engineering, Escola Politécnica, University of São Paulo, São Paulo, Brazil

[c] Université Grenoble Alpes, CNRS, Grenoble INP, Laboratoire SIMAP, F-38000 Grenoble, France

* alastair.marsh@epfl.ch

1 Tricalcium silicate synthesis

Batches of T_1 tricalcium silicate (triclinic polymorph) were synthesized using the 'kilo-scale' method [1]. Reagents of 0.2-0.3 µm fumed silica (S5505, Sigma Aldrich) and calcium carbonate (22300, VWR) were ground and homogenized by wet-grinding with deionized water in a zirconia tumbling ball mill, with zirconia grinding balls. The wet slurry was cast into cylindrical moulds and dehydrated in a 105 °C oven for >72 h. The 'green' cylinders were placed into platinum pan crucibles, and fired in a Borel furnace using a heating rate of 7 °C min^{-1} then held at 1600 °C for 3 h. The cylinders were removed from the furnace and rapidly cooled in front of a fan. The synthesized C_3S consisted of >99.5 wt.% of T_1 tricalcium silicate (C_3S), with trace amounts (<0.5 wt.%) of dicalcium silicate (β C_2S) and free lime (CaO).

2 Grinding and treatment processes

2.1 High-energy grinding

A Siebtechnik disk mill, using a steel grinding vessel and steel grinding rings, was used for the high-energy grinding process. The approximate mass of sample ground in one batch was 62±2 g, corresponding to a single fired cylinder. The fired cylinder was initially crushed using a pestle and mortar to break it down into pieces small enough to fit between the rings of the disk mill (approximately <15 mm diameter). Five drops of isopropanol were added as a grinding aid, following the procedure of Li et al. [1]. Grinding durations used were 3, 6, 24, 60, 120 and 240 s. For samples longer than 30 s, grinding was carried out in intervals of 30 s with a minimal pause, to check that the vessel was still secured in place. Ground samples were stored under vacuum in a desiccator. Volume frequency curves obtained by laser diffraction are shown in Figure S8.

2.2 Low-energy grinding

A Glen Creston McCrone mill, using a plastic vessel and agate cylindrical grinding media, was used for the low-energy grinding process. In order to generate powder sufficiently fine for the McCrone mill, all powder was previously ground for 3 s in a disk mill (following the conditions described above) before subsequent milling in the McCrone mill. 3 g of tricalcium silicate was ground in one batch along with 4 ml of isopropanol. Grinding durations used were 3, 5, 15 and 30 min. Grinding durations were selected, based on the values previously used in [2]. From the curves for specific surface area generated (Figure S1), 15 min grinding in the McCrone mill was identified as being sufficient to achieve a specific surface area approximately the same as that achieved by 15 min grinding in the disk mill. Whilst the 15 min grinding in the McCrone mill did cause some broadening in the X-ray diffraction peaks relative to the sample ground only for 3 s in the disk mill, the extent of broadening was noticeably less compared to the sample ground for 240 s in the disk mill (Figure S2).

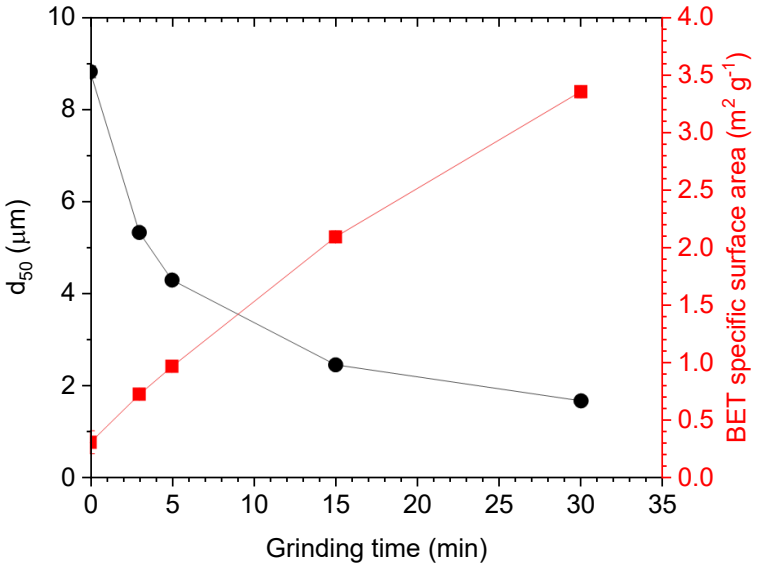

Figure S1: Grinding curves for low-energy milled samples (via McCrone mill). The datapoint at 0 min grinding time corresponds to a sample ground for 3 s in a disk mill, without subsequent grinding in the McCrone mill.

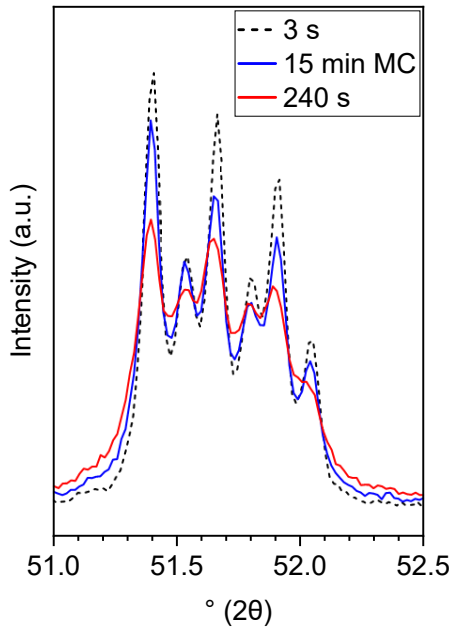

Figure S2: XRD patterns for samples: 3 s in disk mill, 240 s in disk mill, and 3 s in disk mill and subsequent 15 min in McCrone mill (labelled as "15 min MC").

2.3 Annealing

To anneal out defects in the ground tricalcium silicate, samples were annealed by heating in a furnace, with ~10 g of sample placed in a platinum crucible. Samples were heated from room temperature at 20 °C min^{-1}, held and 650 °C for 6 h, and then allowed to cool slowly in the furnace overnight following the same conditions used by Costoya [3].

3 Characterisation of milled powders

3.1 Structural order and amorphous content measurement

X-ray diffraction (XRD) powder patterns were obtained using a Panalytical with a Cu Kα source, operating at 45 kV and 40 mA. Soller slits of 0.04 rad were used for both the incident and diffracted beam path. Incident divergence and antiscatter slits were fixed at 0.5°, and the receiving antiscatter slit was fixed at 1°. Air scattering was reduced using a beam knife. Diffraction patterns were collected over a 2θ range of 5-70 °, with a step size of 0.017 °2θ and a step duration of 0.5 s. The sample stage was rotated at a speed of 30 rpm during measurement. Structure files used were ICSD #4331 for tricalcium silicate (T_1 C_3S) [4], ICSD #81096 for dicalcium silicate (β C_2S) [5], and ICSD #75786 for free lime (CaO) [6].

The amorphous content of the sample was estimated via the internal standard method. 20 wt.% of rutile, TiO_2 (Kronos 2063) was chosen as a suita ble internal standard, following Snellings et al. [7]. The rutile was blended with tricalcium silicate by grinding in a McCrone mill for 1 min; this was deemed to be an acceptable compromise to achieve effective homogenisation of the powder blend, without significantly changing the particle size distribution or structural order of the constituent materials (Figure S1). 0.6±0.005 g of rutile and 2.4±0.005 g of tricalcium silicate were placed into the milling vessel along with 4 ml of isopropanol, and ground for 1 min. The slurry was poured into a petri dish and placed in a 60 °C oven until all the isopropanol had evaporated. An XRD pattern for the 'spiked' sample was then collected using the same XRD measurement parameters as described above. The Rietveld refinement was carried out in Highscore Panalytical software. Rietveld refinement were performed to quantify the mineralogical phases using the following refining parameters: scale factor, zero shift error, cells, and peak shape parameters (W's, V's, and U's) using pseudo-Voigt function. Finally, the preferred orientation was refined for the compounds that tend to orient themselves according to the same crystallographic plane using the spherical harmonics function.

3.2 Physical particle characteristics

The particle size distributions of the ground tricalcium silicate samples were measured via laser diffraction. A Malvern Mastersizer 2000 diffractometer was used, with isopropanol as a dispersal medium. Before measurement, mechanical dispersion using an ultrasonic probe and magnetic stirrer for 5 min was carried out on a dispersion of ~250 mg of powder in 50 ml of isopropanol. Droplets of the dispersion were then added into the diffractomer until an obscuration value of ~13% was achieved. Dispersion unit speed was set to 1700 rpm. Average curves were obtained from a series of ten consecutive measurements of 4 s duration each. Optical parameters used were a refractive index (n) of 1.7, an absorption coefficient of 0.1, and a refractive index (n) of 1.39 for the isopropanol dispersal medium, following guidelines in [8].

BET specific surface area (SSA) was determined from N_2 sorption isotherms. 5±0.5 g of sample was degassed for 16 h at 40 °C under N_2 flow in a Micromeritics Flowprep 060 unit. Isotherms were measured at 77 K using a Micromeritics Tristar II Plus. The Rouquerol validity criteria were used to select datapoints within the range of $p\ p_0^{-1}$ = 0.05-0.3, using a minimum of 5 datapoints for all measurements [9]. N_2 sorption instruments require a minimum total surface area for measurement, which means that samples with low SSA can fall below given physical limitations on the mass of material that can be placed into the sample tube. This is reflected in the larger estimated uncertainties for the DM-3s and DM-6s samples.

Particle morphology was qualitatively assessed via SEM imaging. Ground powder samples were mixed with an epoxy resin (EPOTEK 301), placed in a silicone mould, and then placed under vacuum to remove entrained air. After being left to harden for >24 h, the sample was ground level with silicon carbide grinding paper (1200 grade), and then polished using successive polishing steps using 9, 3 and 1 µm diamond spray (DP Spray-P, Struers). A conductive carbon coating of nominal thickness 15 nm was applied via sputter coating. Images were collected in a FEI Quanta 200 using a backscatter electron detector, using an accelerating voltage of 15 kV, and a working distance of 12.5 mm.

3.3 Raman confocal spectroscopy

Polished sections of the ground powders were prepared using the same procedure described above for scanning electron microscopy, albeit without the carbon coating step.

A Renishaw inVia confocal microscope was used, with a laser wavelength of 532 nm, and a 3000 mm^{-1} grating. Images were recorded using the 100x objective lens. Spectra were measured using a laser power of 50% and a duration of 60 s. Internal calibration was carried out on a silicon standard. The resolution of the laser was approximately ~1µm. Data processing, including baseline correction and cosmic ray removal, was carried out in WIRE 4.4 software. Bands were indexed with reference to [10].

Three types of particles were analysed: coarse particles (> 5 µm diameter) in the 3 s ground sample; coarse samples (> 5 µm diameter) with a typical, dense microstructure in the 240 s ground sample, and large particles (> 20 µm diameter) with a porous microstructure in the 240 s ground sample. At least three particles of each type were analysed. Additional micrographs and spectra from the 240 s ground sample are provided in the Supplementary Results: coarse samples with conventional morphology in Figure S7A,B, and large particles with a porous microstructure in Figure S7C,D.

3.4 Drop calorimetry

The heat of amorphization was determined using drop calorimetry. Pellets of crystalline tricalcium silicate (3 s grinding time) and with maximum amorphous content (240 s grinding time) with a typical weight ranging from 30 to 80 mg were dropped from room temperature into a Setaram MHTC96 calorimeter at 1400 °C. The detailed procedure is reported in [11].

Drop calorimetry measurements include a negative contribution from surface energy effects. The magnitude of these effects is estimated to be in the range of 0.5 - 4 J m^{-2}, with a more commonly occurring range of 1 - 2 J m^{-2} [12]. The BET SSA of these samples ranged from 0.3-1.9 m^2 g^{-1}. Using these values, the most pessimistic estimate for the contribution of surface energy effects is 8 J g^{-1}, with a more realistic estimate of 4 J g^{-1}. This magnitude of both estimated contributions is much smaller than the uncertainty in the measurements themselves (± 30 J g^{-1}) and also much smaller than the difference in mean values between the 3 s (1451.4 J g^{-1}) and 240 s (1532.1 J g^{-1}) ground samples. Therefore, for these samples we believe that the contribution of surface energy effects is negligible.

4 Measurement of hydration kinetics

Pastes were prepared by mixing 5.00±0.05 g of tricalcium silicate with 3.00±0.05 g of deionized water, to give a water/solids ratio of 0.6. The mixture was manually mixed with a spatula for 30 s to ensure all the powder was wetted, followed by 2 min mixing using an IKA Ministar 20 high-shear mixer and flat plate mixer attachment at 1600 rpm. 5±0.05 g of paste was cast into a glass ampoule, and placed inside a TAM Air isothermal calorimeter (Gen V) at 20 °C. Reference ampoules consisting of 2.44 g of water were placed into the reference channels. Measurements were collected for 7 d. A baseline correction was carried out in the TAM Assistant software, using a linear interpolation of baselines collected for 1 h before and after the measurement.

To measure the activation energy of hydration, additional isothermal calorimetry measurements were carried out at 30 °C and 40 °C, using the same paste preparation procedure described above. Following the 'single linear approximation' method [13], the tangent of the linear section of the hydration peak was extracted from the cumulative heat curves; given the simple phase composition of these samples, this was calculated objectively via taking the tangent value at the peak of the first derivative (i.e. the heat flow curve). An Arrhenius plot was constructed using these values (Figure S3); activation energy was then calculated from the gradient of the linear best-fit line, using Equation S1.

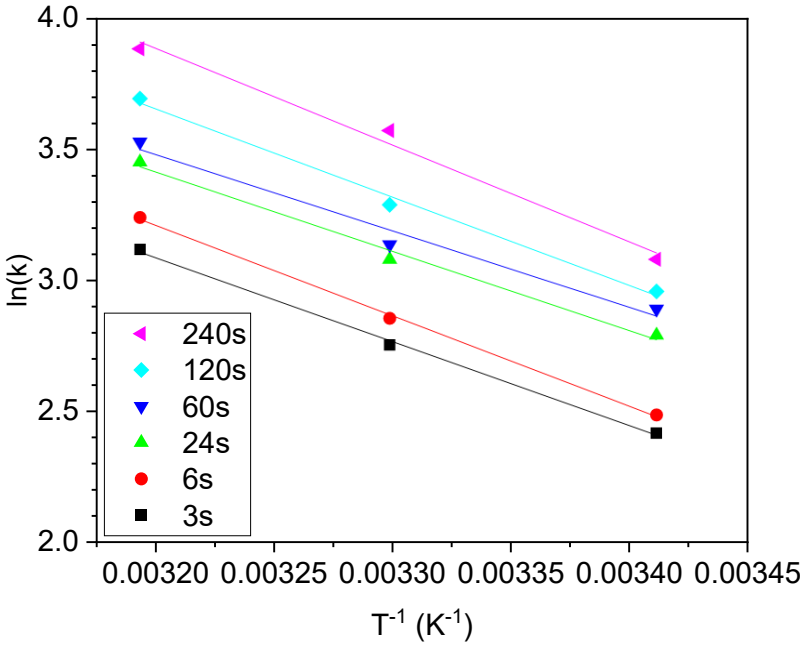

Figure S3: Arrhenius plot constructed using values from the isothermal calorimetry measurements carried out at 20, 30 and 40 °C.

Equation S1: Arrhenius equation used to calculate apparent activation energy (E_A) from the Arrhenius plot in Figure S3. k (J g^{-1} h^{-1}) is the rate constant, corresponding to the tangent of the heat flow curve at its linear stage during the acceleration period; A is the pre-exponential factor

corresponding to the y-intercept on the Arrhenius plot; R is the gas constant; T (K) is the temperature at which the isothermal calorimetry measurement was obtained.

$$ln(k) = ln(A) - \frac{E_A}{R}\left(\frac{1}{T}\right)$$

5 Modelling of hydration kinetics

Modelled hydration curves were generated in Matlab, using the 'needle growth' model developed by Ouzia and Scrivener [14]. This model is based on a first principles approach of modelling the growth of needles of C-S-H, rather than empirically fitting parameters.

The following values were used (Table S1), selected as mid-point values provided in Table 1 of [14]. A good fit was obtained for the 3 ground sample (Figure S4); accordingly, the same values were used to model all other grinding times too. Particle size radii, R, was varied according to the measured volume frequency curves obtained via laser diffraction (ESI 3.2). For later ageing times, the fit between the modelled and measured curves was less good (Figure S5).

Table S1: Values for parameters that were fixed for all grinding times.

Model parameter	**Symbol / abbreviation**	**Value**
Form factor	F	1/3
Roughness factor	Rou	2
Final length	l_{max}	0.35 µm
Final radius	r_{max}	0.042 µm
Characteristic growth time	t_c	4 h
Characteristic nucleation rate	K_n	40 $\mu m^{-2}\ h^{-1}$
Characteristic nucleation transition time	t_n	1 h
Nucleation starting time	t_{start}	1 h
Nucleation stopping time	t_{stop}	5 h
Heat of reaction	$\Delta_r H$	524 J g^{-1}
C_3S density	M_{C3S}	3.1 g cm^{-3}

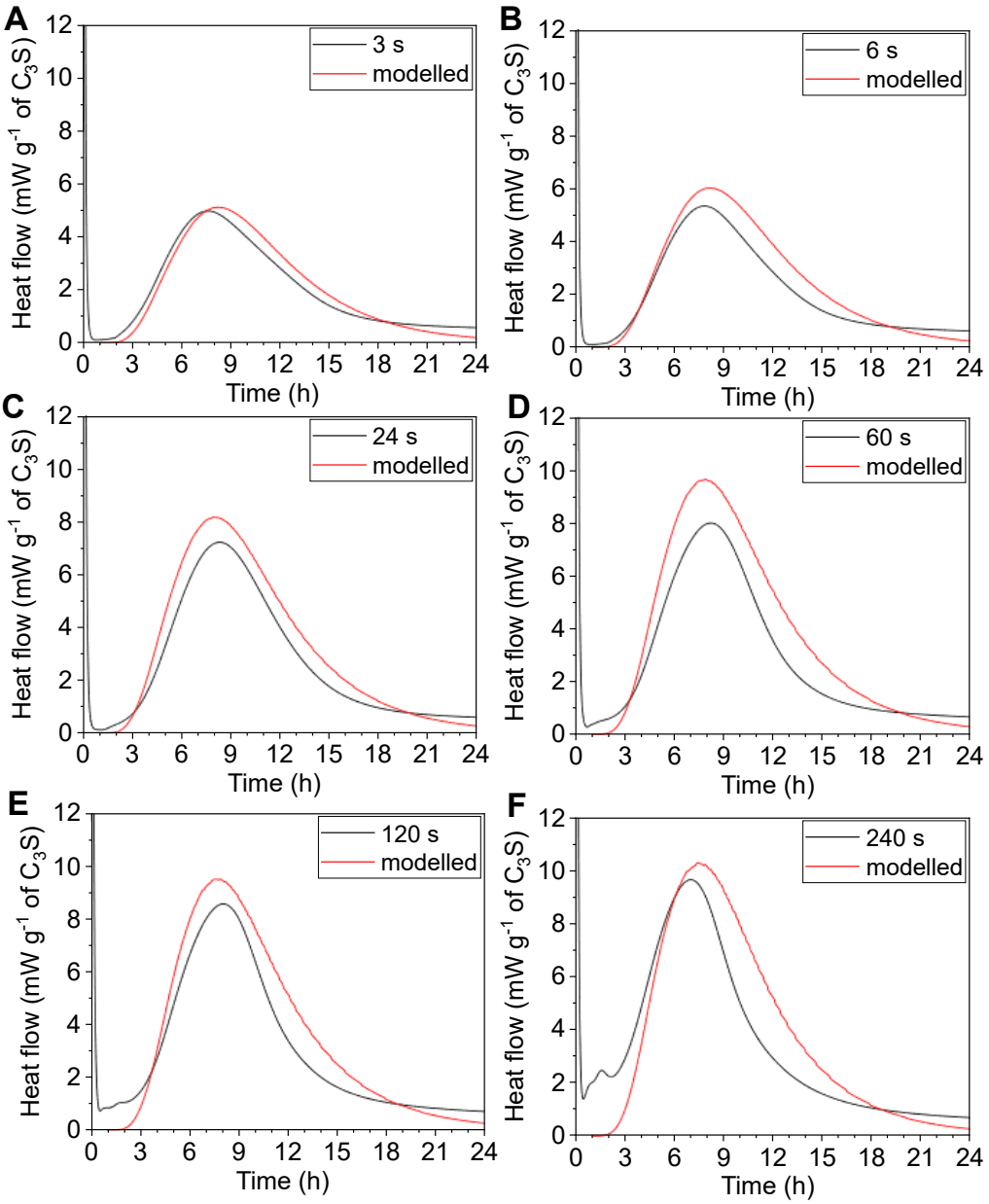

Figure S4: A comparison of the measured and modelled hydration curves for the sample ground for A) 3 s; B) 6 s; C) 24 s; D) 60 s; E) 120 s; F) 240 s.

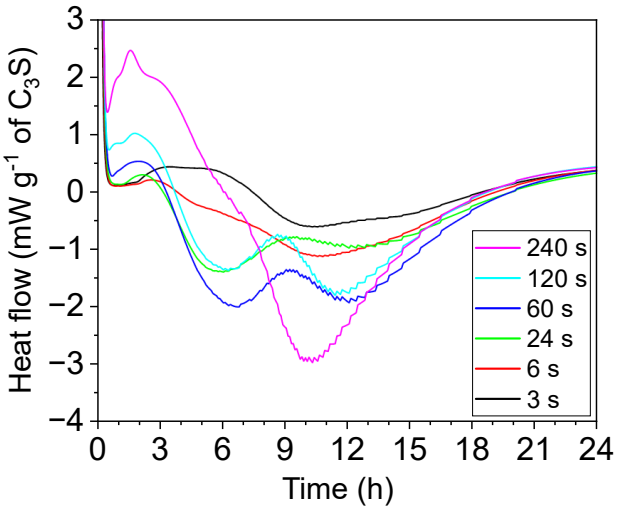

Figure S5: Residual curves, showing the difference between the measured and modelled hydration heat flow curves.

6 Additional results

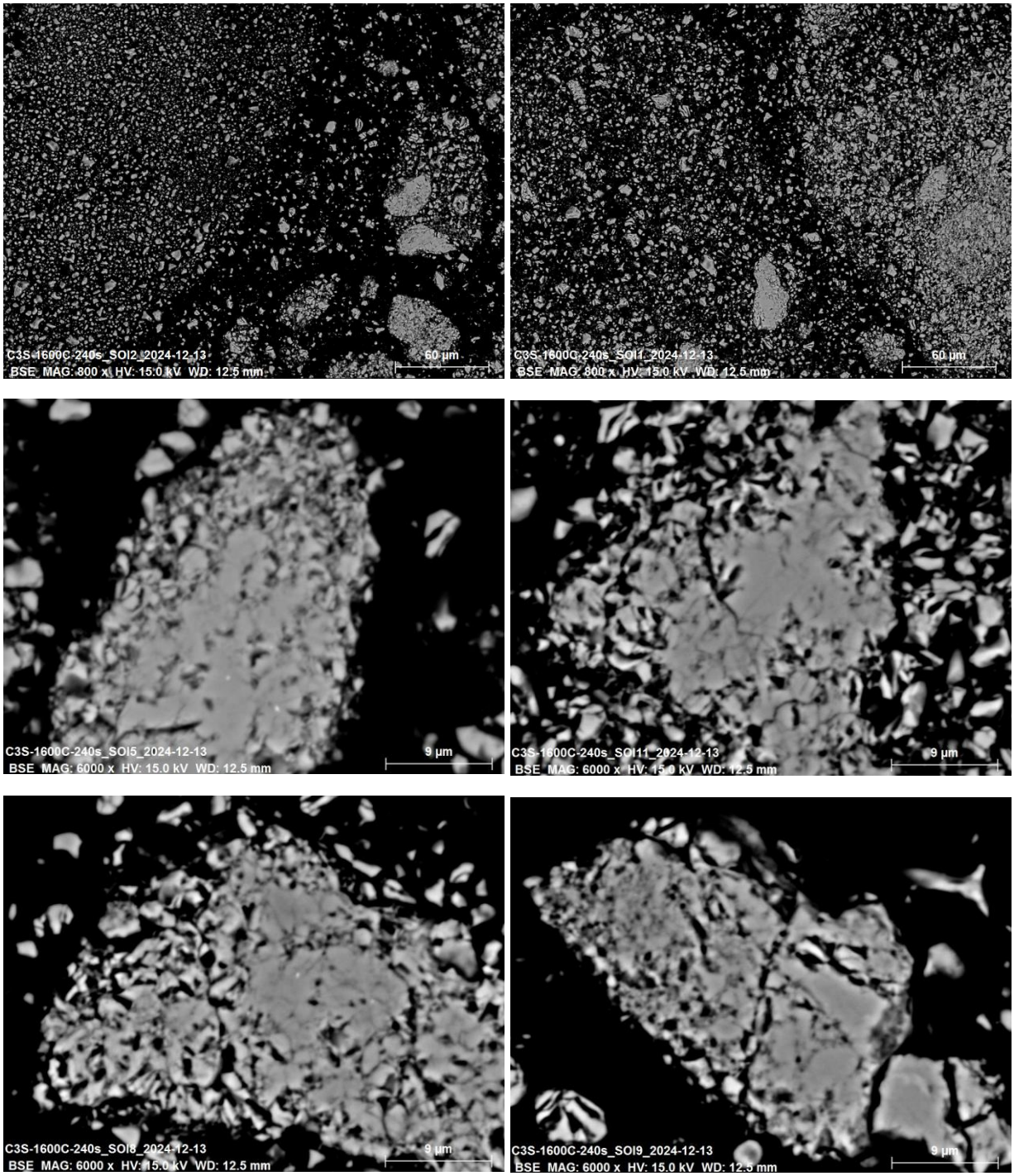

Figure S6: Backscatter electron images of the tricalcium silicate ground for 240 s, obtained via scanning electron microscopy.

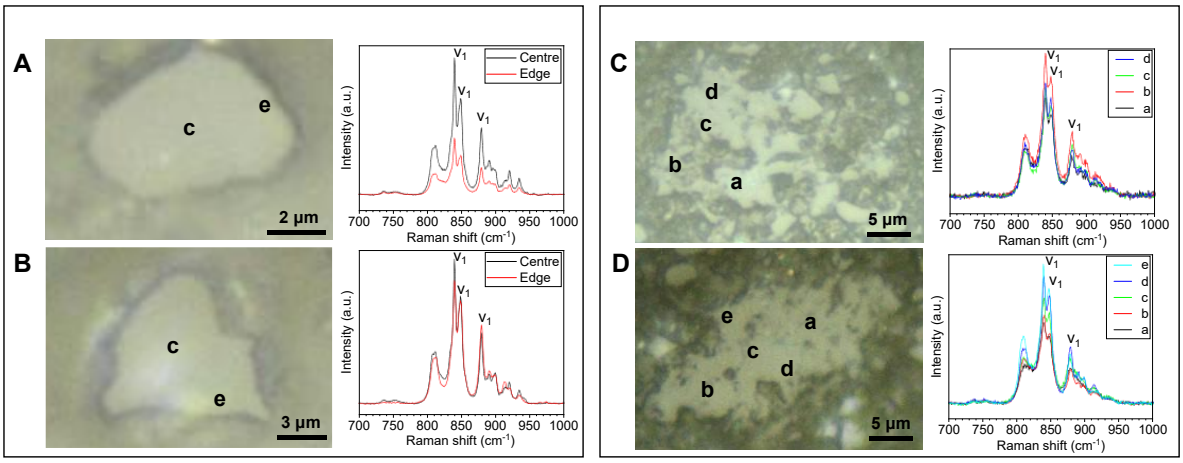

Figure S7: Additional optical microscope images and Raman spectra for individual particles of tricalcium silicate. All particles are from the 240 s ground sample. Images A,B) show coarse particles (> 5 µm diameter) with a typical, dense microstructure. Images C,D) show large particles (> 20 µm diameter) with a porous microstructure. For A-B), the "c" and "e" annotations represent the centre and edge regions, representing the spectra. For C-D), the letters simply identify different regions within those particles. v_1 denotes the position of $v_1(SiO_4)^{4-}$ bands.

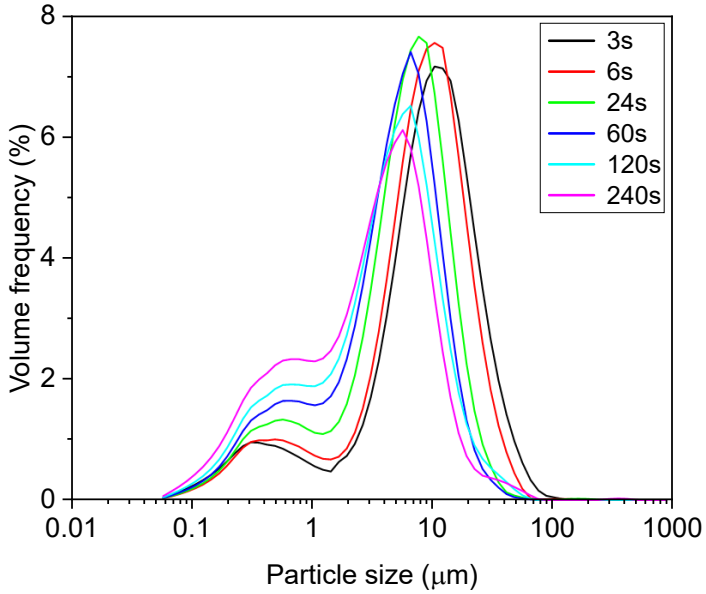

Figure S8: Volume frequency curves obtained by laser diffraction, for the tricalcium silicate samples ground for 2 to 240 s using high-energy grinding.

References

1. X. Li, A. Ouzia and K. Scrivener, *Cement and Concrete Research*, 2018, **108**, 201-207.
2. S. Ravaszova and K. Dvorak, *IOP Conference Series: Materials Science and Engineering*, 2018, **385**, 012044.
3. M. M. Costoya Fernández, *Effect of particle size on the hydration kinetics and microstructural development of tricalcium silicate*, EPFL, 2008.
4. N. Golovastikov, *Sov. Phys. Crystallogr.*, 1975, **20**, 441-445.
5. W. Mumme, *N. Jb. Miner. Abr.*, 1995, **169**, 35-68.
6. Q. Huang, O. Chmaissem, J. J. Capponi, C. Chaillout, M. Marezio, J. L. Tholence and A. Santoro, *Physica C: Superconductivity*, 1994, **227**, 1-9.
7. R. Snellings, A. Bazzoni and K. Scrivener, *Cement and Concrete Research*, 2014, **59**, 139-146.
8. M. Palacios, H. Kazemi-Kamyab, S. Mantellato and P. Bowen, in *A practical guide to microstructural analysis of cementitious materials*, eds. K. Scrivener, R. Snellings and B. Lothenbach, CRC Press, Boca Raton, FL, 2016, DOI: 10.1201/b19074, pp. 445-480.
9. M. Thommes, K. Kaneko, A. V. Neimark, J. P. Olivier, F. Rodriguez-Reinoso, J. Rouquerol and K. S. W. Sing, 2015, **87**, 1051-1069.
10. V. Timón, D. Torrens-Martin, L. J. Fernández-Carrasco and S. Martínez-Ramírez, *Cement and Concrete Research*, 2023, **169**, 107162.
11. W. Abdul, C. Mawalala, A. Pisch and M. N. Bannerman, *Cement and Concrete Research*, 2023, **173**, 107309.
12. A. Navrotsky, *Journal of the American Ceramic Society*, 2014, **97**, 3349-3359.
13. J. L. Poole, K. A. Riding, K. J. Folliard, M. C. G. Juenger and A. K. Schindler, *ACI Materials Journal*, 2007, **104**, 303-311.
14. A. Ouzia and K. Scrivener, *Cement and Concrete Research*, 2019, **115**, 339-360.